Eighth Hungarian Conference on Computer Graphics and Geometry, Budapest, 2016

Anatomy-based Regularization Methods for Dynamic PET Reconstruction

Ágota Kacsó and László Szirmay-Kalos

Budapest University of Technology and Economics (e-mail: szirmay@iit.bme.hu)

Abstract

This paper examines and compares regularization methods for direct parametric dynamic PET reconstruction, when the space-time activity function needs to be recovered from measurements. In binned mode reconstruction, the measurement time is decomposed to frames and events are binned. In order to mimic high-speed phenomena, frames must be short, thus the number of events in a frame is very low, making frame-wise reconstruction impossible. To attack this problem, regularization is needed that enforces smoothness both in the temporal and spatial domains. For temporal regularization, different kinetic models are used. For spatial regularization, we can subtract a penalty term from the likelihood of the measured data that penalizes unacceptable solutions, or the reconstruction can be filtered in every iteration to project the actual estimate into the subspace of acceptable solutions. The objective of this paper is to analyze these options and compare their effectiveness.

1. Introduction

In dynamic Positron Emission Tomography (PET), we measure how the density of a radiotracer changes in time at different voxels of the examined object, thus dynamic tomography reconstructs a space-time density $x_V(t)$. The spatial variation of the density is defined on a grid [20, 2, 3, 4, 26, 15], for example, in voxels. Using the space-time density, the expected number of radioactive decays in voxel V in differential time $\mathrm{d}t$ is $x_V(t)\mathrm{d}t$. The positron emitted at a decay annihilates with an electron generating two oppositely directed gamma-photons, which might be detected by the tomograph. A PET/CT system collects the *events* of simultaneous photon incidents in detector pairs, called *Line Of Response* or *LOR*. The measurement time is decomposed into finite time intervals, called frames $\Delta t_1, \ldots, \Delta t_{N_T}$ with interval centers $t_1, \ldots, t_T$, and events are binned in frames. We denote the number of events in LOR L and frame T by $y_{L,T}$.

If fast dynamic changes are to be recovered, frames must be short and consequently the number of events in a frame is rather low. This means that reconstruction done independently in frames is either impossible or leads to very noisy data. To attack this problem, regularization is needed that enforces the smoothness both in the temporal and the spatial domains.

2. Dynamic PET reconstruction

The state of the art and previous work on direct estimation of kinetic parametric images for dynamic PET are surveyed in review article [28].

The event rate $\lambda_L(t)$ in LOR L at time t is the sum of the contributions of all voxels in the volume at this time:

$$\lambda_L(t) = \sum_{V=1}^{N_V} \mathbf{A}_{LV} x_V(t)$$

where *system matrix* $\mathbf{A}_{L,V}$ expresses the probability that a decay in voxel V generates an event in LOR L.

During iterative *Expectation Maximization* (ML-EM) reconstruction [16], unknown coefficients are found to maximize the probability of the actually measured data. Assuming that the measured number of hits in LOR L in time interval Δt_T follows a Poisson distribution and is statistically independent of other LORs and frames, the log-likelihood of the current measurement is

$$\log \mathcal{L} = \sum_L \sum_T \left(y_{L,T} \log \lambda_L(t_T) - \lambda_L(t_T) \Delta t_T \right). \qquad (1)$$

The high variance of the involved random variables makes the optimization process fit the solution to noise, resulting in unacceptably high variation reconstructions. The tempo-

ral and spatial variation of the solution must be kept under control, which is the responsibility of regularization.

2.1. Temporal regularization

For temporal regularization, we assume that the time activity function of voxel V can be expressed by a common *kinetic model*

$$x_V(t) = F(\theta_V, t),$$

where spatially dependent properties are encoded in a low dimensional vector of parameters θ. Such models can be based on the mathematical description of the biological/chemimal processes or on compartment analysis [5, 30, 29].

2.2. Spatial regularization with a penalty term

One possibility to impose spatial regularization is to include a penalty term $R(\theta)$ into the optimization target function. Thus, we find the extremum of the following functional:

$$E(\theta) = \log \mathcal{L}(\theta) - R(\theta). \tag{2}$$

The penalty term should be high for unacceptable solutions and small for acceptable ones. Standard regularization methods like Tikhonov regularization and Truncated Singular Value Decomposition (TSVD) assume the data set to be smooth and continuous, and thus enforce these properties during reconstruction. However, the typical data in PET reconstruction are different, there are sharp features that should not be smoothed with the regularization method. We need a penalty term that minimizes the unjustified oscillation without blurring sharp features. An appropriate penalty term is the *total variation* (TV) of the solution [14, 11, 10, 12]. Total variation regularization may create stair-like artifacts, which can be reduced by Bregman iteration [23].

The inclusion of the anatomic information into spatial regularization is straightforward, smoothness should be imposed only inside anatomically homogeneous regions but not on their boundaries [1].

2.3. Method of sieves

In this approach, the optimization target is not modified, but the iterated approximation is filtered in each iteration step. Several authors proposed the inclusion of a voxel space filtering step in the reconstruction loop [17, 9] and it turned out that it is equivalent to the method of sieves that seeks to constrain the EM solution to a subspace of all possible solutions [18, 19, 27]. The objective of filtering is to find an acceptable solution that is close to the solution proposed by the iteration. Filtering can also exploit anatomic information gathered by a CT or an MR [24].

2.4. The proposed method

The reconstruction means the solution of the optimization problem of Equation 2. The optimization target has an extremum where all partial derivatives are zero:

$$\frac{\partial E(\theta)}{\partial \theta_{V,P}} = 0.$$

Computing the partial derivatives, we obtain

$$\left(\sum_L \mathbf{A}_{L,V}\right) \sum_T \left.\frac{\partial F}{\partial \theta_{V,P}}\right|_{t_T} \left(\frac{x_{V,T}(\theta)}{F(\theta_V, t_T)} - \Delta t_T\right) - \frac{\partial R}{\partial \theta_{V,P}} = 0, \tag{3}$$

where $x_{V,T}$ is the result of a static forward projection and back projection taking the data from frame T:

$$\lambda_{L,T} = \sum_{V'} \mathbf{A}_{L,V'} F(\theta_{V'}, t_T)$$

$$x_{V,T} = F(\theta_V, t_T) \cdot \frac{\sum_L \mathbf{A}_{L,V} \frac{y_{L,T}}{\lambda_{L,T}}}{\sum_L \mathbf{A}_{L,V}}.$$

In this equation kinetic model F depends on unknown parameter vector of the given voxel θ_V, while $x_{V,T}$ and R depend on the parameter vectors of all voxels. Additionally, $x_{V,T}$ is the only factor that is affected by the elements of the system matrix. Thus, if $x_{V,T}$ and R were known, then the computation could be decoupled for different voxels and can be made independent of the huge system matrix.

To achieve this, a subiteration is included into the main iteration solution of this equation. In the subiteration expensive terms like $x_{V,T}$ and R are not re-evaluated, they are updated just in the main iteration steps, which update $x_{V,T}$ and R. The task of the subiteration is the solution of the following function for $\theta_V^{(n+1)}$:

$$\left(\sum_L \mathbf{A}_{L,V}\right) \sum_T \left.\frac{\partial F(\theta_V^{(n+1)})}{\partial \theta_{V,P}}\right|_{t_T} \left(\frac{x_{V,T}(\theta^{(n)})}{F(\theta_V^{(n+1)}, t_T)} - \Delta t_T\right) -$$

$$\frac{\partial R(\theta_V^{(n)})}{\partial \theta_{V,P}} = 0. \tag{4}$$

Assuming that $x_{V,T}$ is constant, Equation 4 describes just a single voxel, and can thus be solved independently for all voxels. We use the *Iterative Coordinate Descent* algorithm for the solution, which leads to set of parameters for this particular voxels, which define a time activity curve $F(\theta_V, t)$ that fits to $x_{V,T}$.

For the regularization, we consider the options of temporal regularization via kinetic models, spatial regularization with the penalty of the total variation of the activity, the penalty of the total variation of the parameters, filtering the activity, and filtering the parameters.

2.5. Temporal regularization with various kinetic models

Time activity $F(\theta,t)$ depends on the concentration $C(\theta,t)$ of the radiotracer and on the known decay constant λ of the radiotracer:

$$F(\theta,t) = C(\theta,t)\exp(-\lambda t).$$

The concentration is searched in a finite function series form defined by parameter vector θ. The basis functions of this approximation can be general, like B-splines of Mixture of Gaussians, or can be derived from the biological models of the diffusion.

2.5.1. Mixture of Gaussians

In this case, the basis functions are temporal Gaussians defined by fixed time value t_P and temporal deviation σ_P:

$$C(\theta,t) = \sum_P a_P \cdot \frac{\exp\left(-\frac{(t-t_P)^2}{2\sigma_P^2}\right)}{\sqrt{2\pi}\sigma_P}, \quad \theta = (a_1,\ldots,a_{N_P})$$

Deviation σ_P should be selected to guarantee that the drop to the next time values is not too large.

2.5.2. Spectral method

In spectral method, we also assume the knowledge of the blood input function $C_p(t)$ that describes the radiotracer concentration in the blood from where diffusion can start. The basis functions are convolutions of exponentials of predefined exponents α_P and the known blood input function:

$$C(\theta,t) = \sum_P a_P \cdot \alpha_P \exp(-\alpha_P t) * C_p(t), \quad \theta = (a_1,\ldots,a_{N_P}).$$

The *Binding Potential* (BP) can be directly computed from the coefficients of the spectral method:

$$BP = -1 + \sum_{P=1}^{N_P} a_P$$

2.5.3. Patlak method

The Patlak method is appropriate for the case of irreversible compartment at steady state, when the two basis functions are the blood input function and its integral:

$$C(\theta,t) = a_1 \int_0^t C_p(\tau)\mathrm{d}\tau + a_2 C_p(t), \quad \theta = (a_1,a_2).$$

We assume that the steady state is reached when C_p starts to decrease. Parameter a_1 is proportional to the metabolic rate.

2.5.4. Relative equilibrium plot

The Relative Equilibrium Plot is a modified version of the Logan Plot and can be used to describe reversible tracers at steady state. The basis functions are the blood input function and its negative derivative:

$$C(\theta,t) = a_1 C_p(t) - a_2 \frac{\mathrm{d}C_p(t)}{\mathrm{d}t}, \quad \theta = (a_1,a_2).$$

Due to the steady state assumption, this model is valid when t is in the range where $C_p(t)$ is already decreasing thus its derivative is negative. The binding potential can be computed from a_1 as $BP = a_1 - 1$.

2.5.5. Two-tissue-compartment model

The two-tissue-compartment model is based on the solution of differential equations describing material exchange between compartments.

$$C(\theta,t) = a_1 \cdot \alpha_1 \exp(-\alpha_1 t) * C_p(t) + a_2 \cdot \alpha_2 \exp(-\alpha_2 t) * C_p(t),$$

$$\theta = (a_1,a_2,\alpha_1,\alpha 2).$$

2.6. Spatial regularization with penalizing the total variation

Total variation can be calculated for the reconstructed activity function $x_V(t)$:

$$TV(x) = \int |\nabla x| \mathrm{d}v \approx$$

$$\sum_V \sqrt{(x_{Vr}-x_V)^2 + (x_{Vu}-x_V)^2 + (x_{Vf}-x_V)^2}$$

assuming that voxels are cubic and at unit distance and denoting the right, upper and front neighbors of voxel V by Vr, Vu, and Vf, respectively.

Alternatively, we can obtain the weighted sum of variations of individual parameters:

$$TV(\theta) = \sum_P \rho_P \int |\nabla \theta_P| \mathrm{d}v$$

where ρ_P is the weight of parameter P.

2.7. Spatial filtering

We apply a Gaussian filtering scheme separately for the activity [9, 8, 13] in the first alternative and for each parameter in the second.

For each voxel, the activities in the neighboring voxels of the same anatomic regions are taken and summed having weighted by a distance dependent Gaussian $G(V',V)$. The sum of weighted parameter values is finally divided by the sum of weights, and the result replaces the original unfiltered parameter value:

$$\hat{x}_V = \frac{\sum_{V'} x_{V'} G(V',V)}{\sum_{V'} G(V',V)}$$

where weight $G(V',V)$ is the Gaussian of the distance between the centers of voxels V and V' if these voxels belong to the same anatomic structure and zero otherwise.

In case of parametric filtering, the same procedure is executed for each voxel and parameter.

$$\hat{\theta}_{V,P} = \frac{\sum_{V'} \theta_{V',P} G(V',V)}{\sum_{V'} G(V',V)}.$$

3. Results

To evaluate the proposed alternatives, we use a 2D brain model measured in a 2D PET [22] where the system matrix can be precisely computed (Fig. 1). The simulation has been executed with the Two-tissue-compartment model. In this case, the Patlak and the Relative equilibrium plot are not applicable so only the Mixture of Gaussian, Spectral, and the Two-tissue-compartment models are taken as reconstruction kinetic models. Both the Mixture of Gaussian and the Spectral method use four basis functions, i.e. have four parameters similarly to the Two-tissue-compartment model. Thus the memory footprints of the methods to be compared are identical. We defined 100 time frames and executed 10 iterations.

Figures 2 and 3 compare the reconstructions obtained with about 8k hits in total, Figures 4 and 5 with about 16k hits, Figures 6 and 7 with about 80k hits, and finally Figures 8 and 9 with about 160k hits. As the number of LORs is 2k, the average number of hits per LOR is just 4 when 8k hits are considered, and as we used 100 frames, the average number of hits in a LOR in a single frame is only 0.04 for the lowest statistics measurement. We provide time activity curves showing the average of the voxels in ROIs and also the standard deviation. Reconstruction results are shown at $t = 1$ when the activity at both ROIs are maximal.

With higher number of hits the noise level of the measurement decreases, so we expect a similar effect on the reconstruction. For all measurements, we can observe that the Spectral method is better than the Mixture of Gaussian, and the Two-tissue-compartment model is better than any of the other two. However, all three methods can be significantly improved by parameter space filtering.

Figures 10 and 11 compare the discussed regularization options. Note that filtering is generally better than adding a penalty term, and filtering the measured LORs performed poorly.

4. Conclusions

In this paper we examined regularization strategies for the problem of dynamic PET reconstruction when the total activity in a region of interest needs to be reconstructed as a function of time. Regularization must be done in the domain of time where a proper time activity model should be chosen, and also in space, which is possible either by filtering

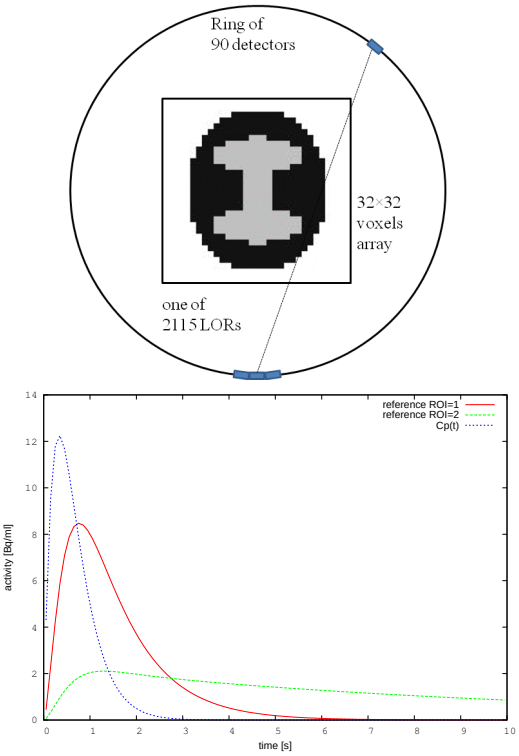

Figure 1: *2D tomograph model: The detector ring contains 90 detector crystals and each of them is of size 2.2 in voxel units and participates in 47 LORs connecting this crystal to crystals being in the opposite half circle, thus the total number of LORs is* $90 \times 47/2 = 2115$. *The voxel array to be reconstructed is in the middle of the ring and has* 32×32 *resolution, i.e. 1024 voxels. The lower image shows the blood input function and the simulated time activity curves in the gray matter (ROI 2) and white matter (ROI 1) of the brain.*

or by adding the penalty term. We concluded that simultaneous temporal and spatial regularization allow accurate reconstructions of very low statistics measurements. According to our experience, spatial filtering outperforms the penalty term spatial regularization and naive approaches like filtering the measured data do not help. In our future work, these algorithms will be integrated into the GPU based fully-3D Teratomo system [6, 7, 25].

Acknowledgement

This work has been supported by OTKA K–104476 and VKSZ-14 PET/MRI 7T projects.

References

1. Chan C., Fulton R., Feng D. D., and Meikle S. Regularized image reconstruction with an anatomically adaptive prior for

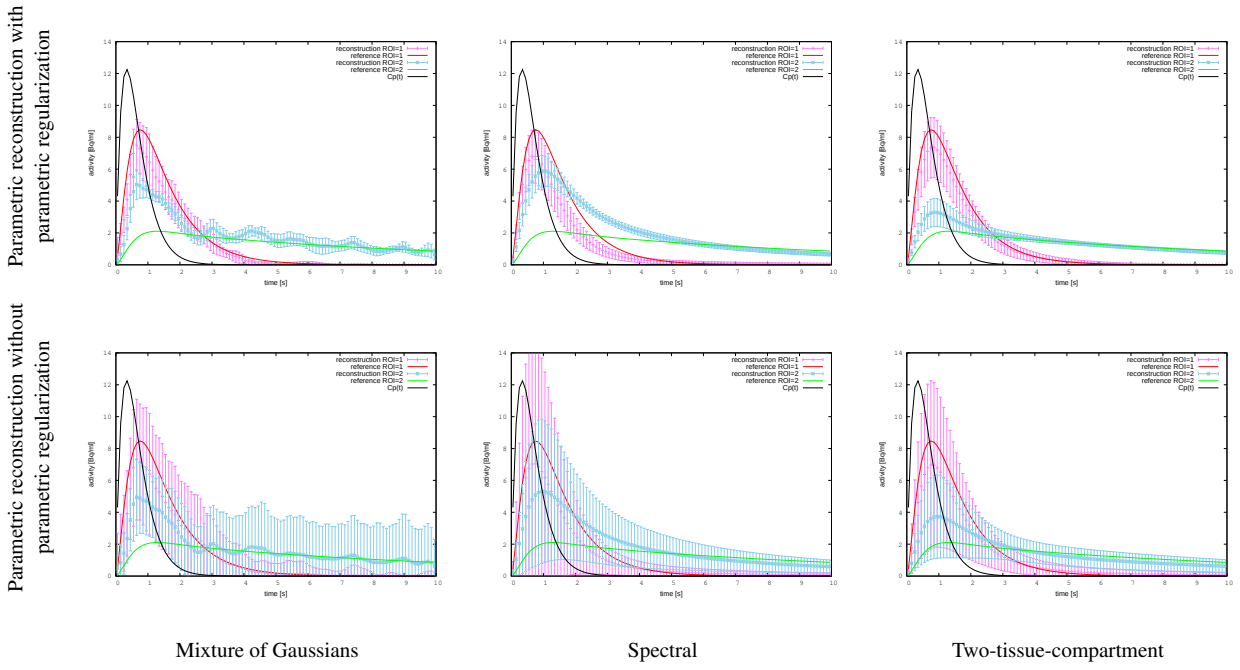

Figure 2: *Time activity functions of voxels in different ROIs, the average and the standard deviation are depicted, the total number of hits is 8k.*

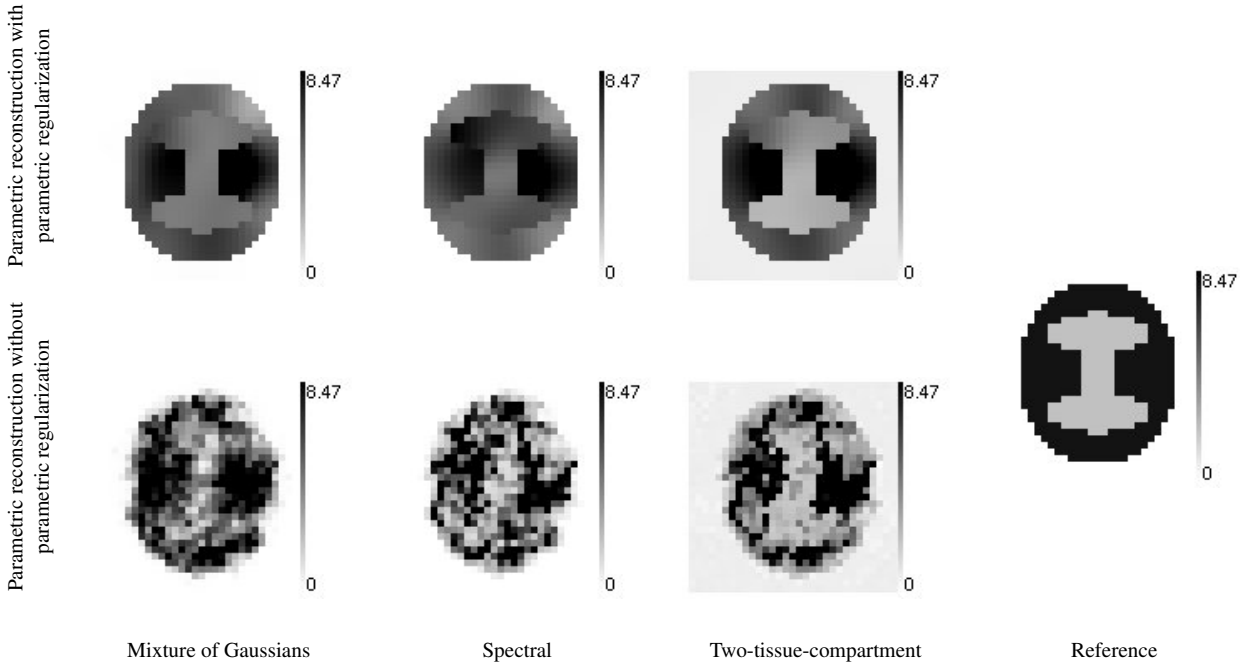

Figure 3: *Examples of reconstructed spatial activity at* $t = 1$*, when the total number of hits is 8k.*

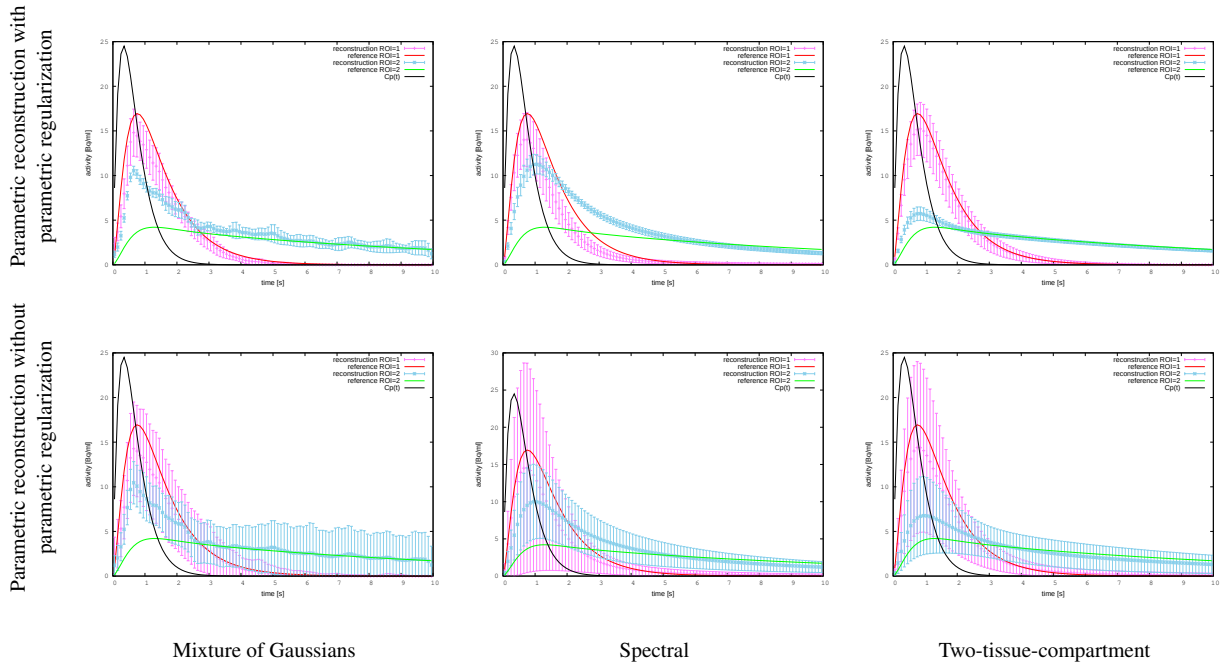

Figure 4: *Time activity functions of voxels in different ROIs, the average and the standard deviation are depicted, the total number of hits is 16k.*

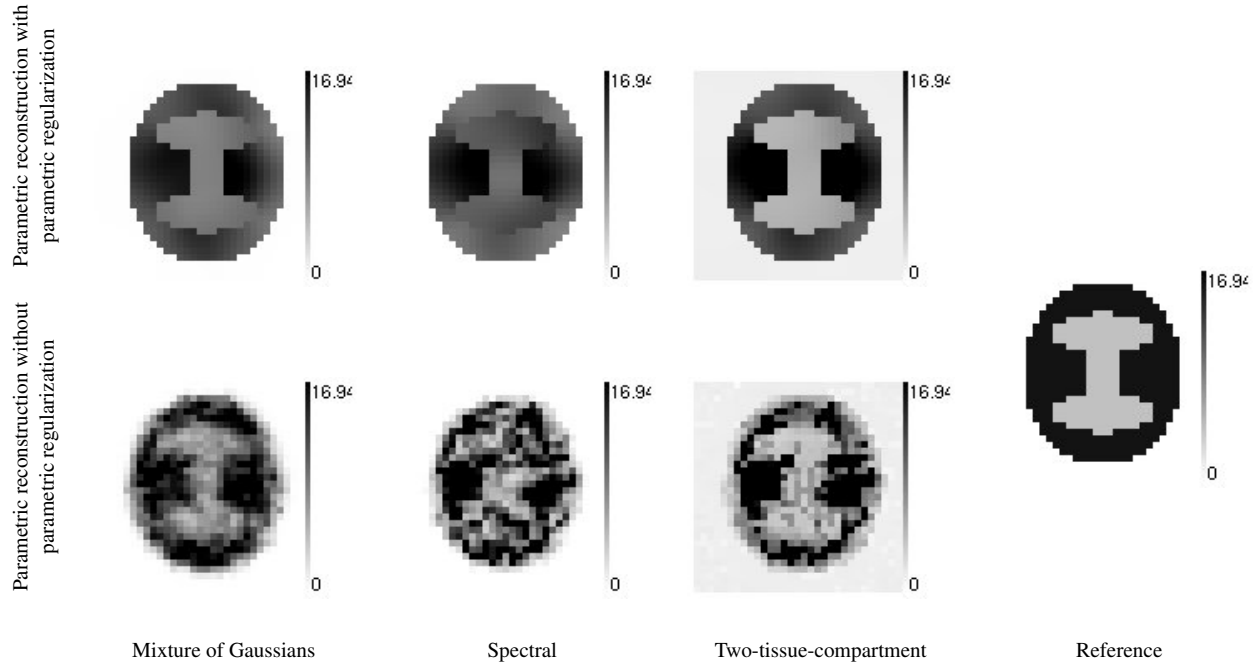

Figure 5: *Examples of reconstructed spatial activity at* $t = 1$*, when the total number of hits is 16k.*

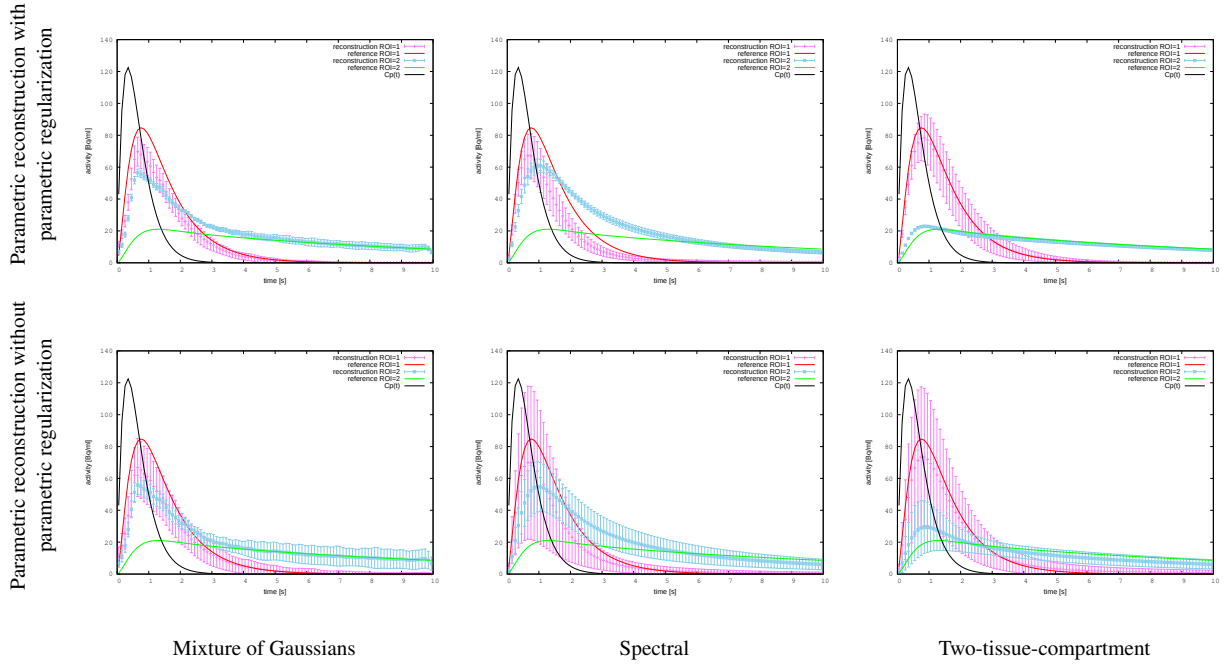

Figure 6: *Time activity functions of voxels in different ROIs, the average and the standard deviation are depicted, the total number of hits is 80k.*

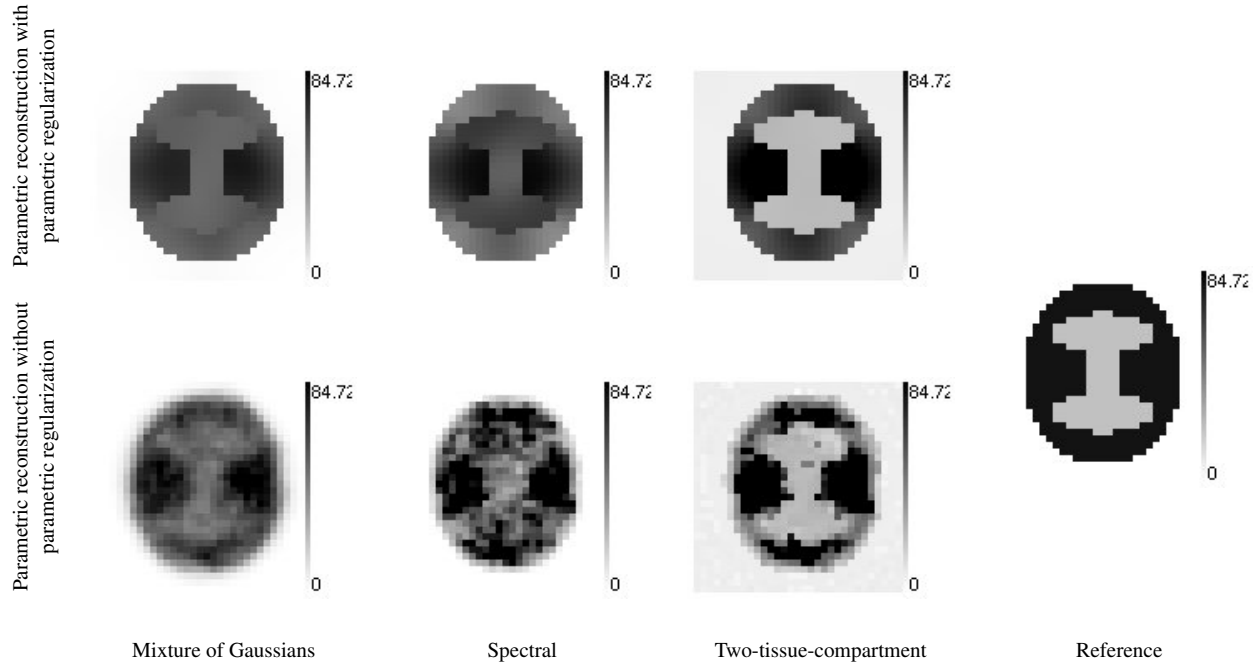

Figure 7: *Examples of reconstructed spatial activity at* $t = 1$*, when the total number of hits is 80k.*

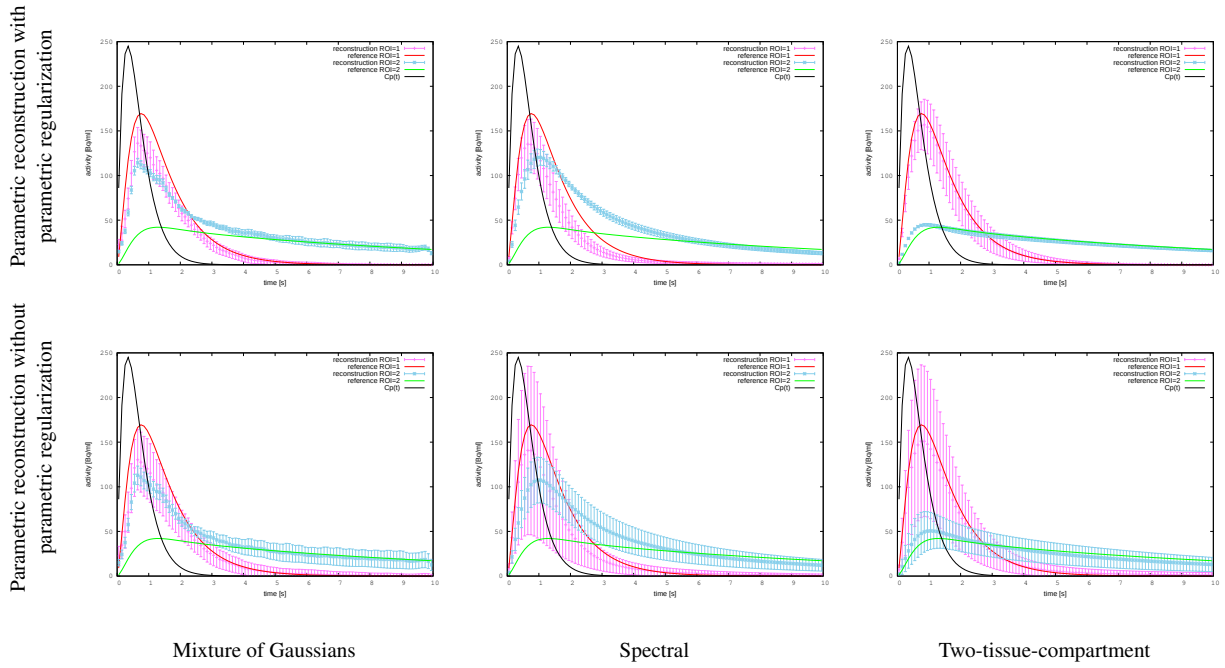

Figure 8: *Time activity functions of voxels in different ROIs, the average and the standard deviation are depicted, the total number of hits is 160k.*

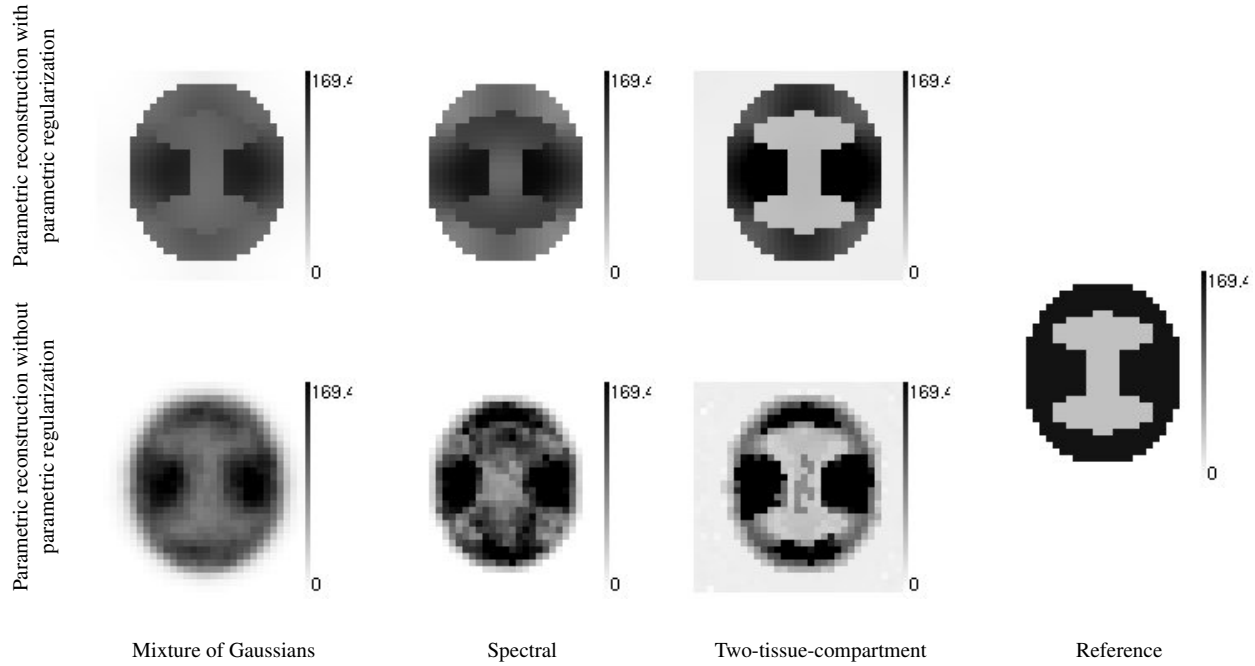

Figure 9: *Examples of reconstructed spatial activity at* $t = 1$*, when the total number of hits is 160k.*

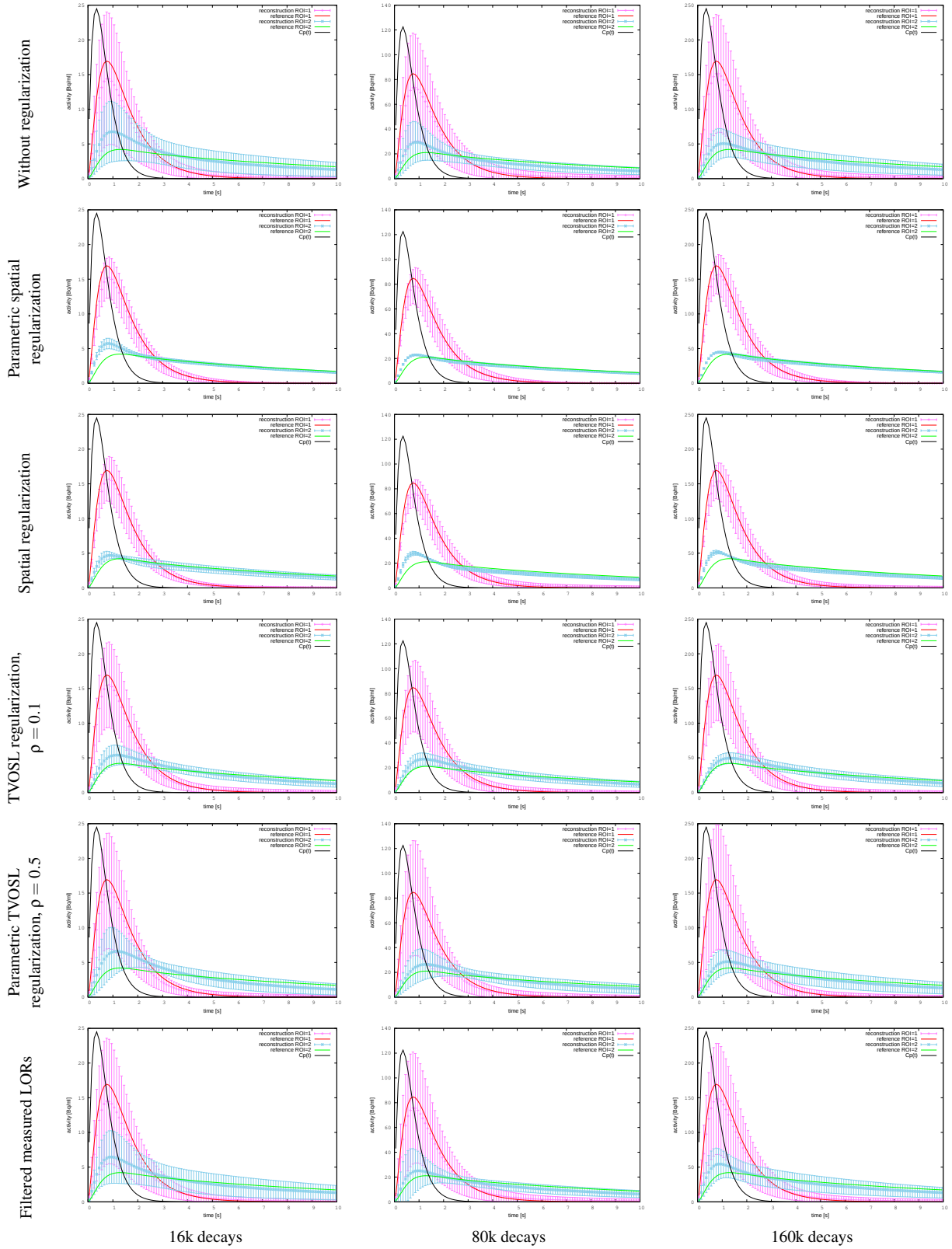

Figure 10: *Comparison of different regularization options for the two-tissue compartment model*

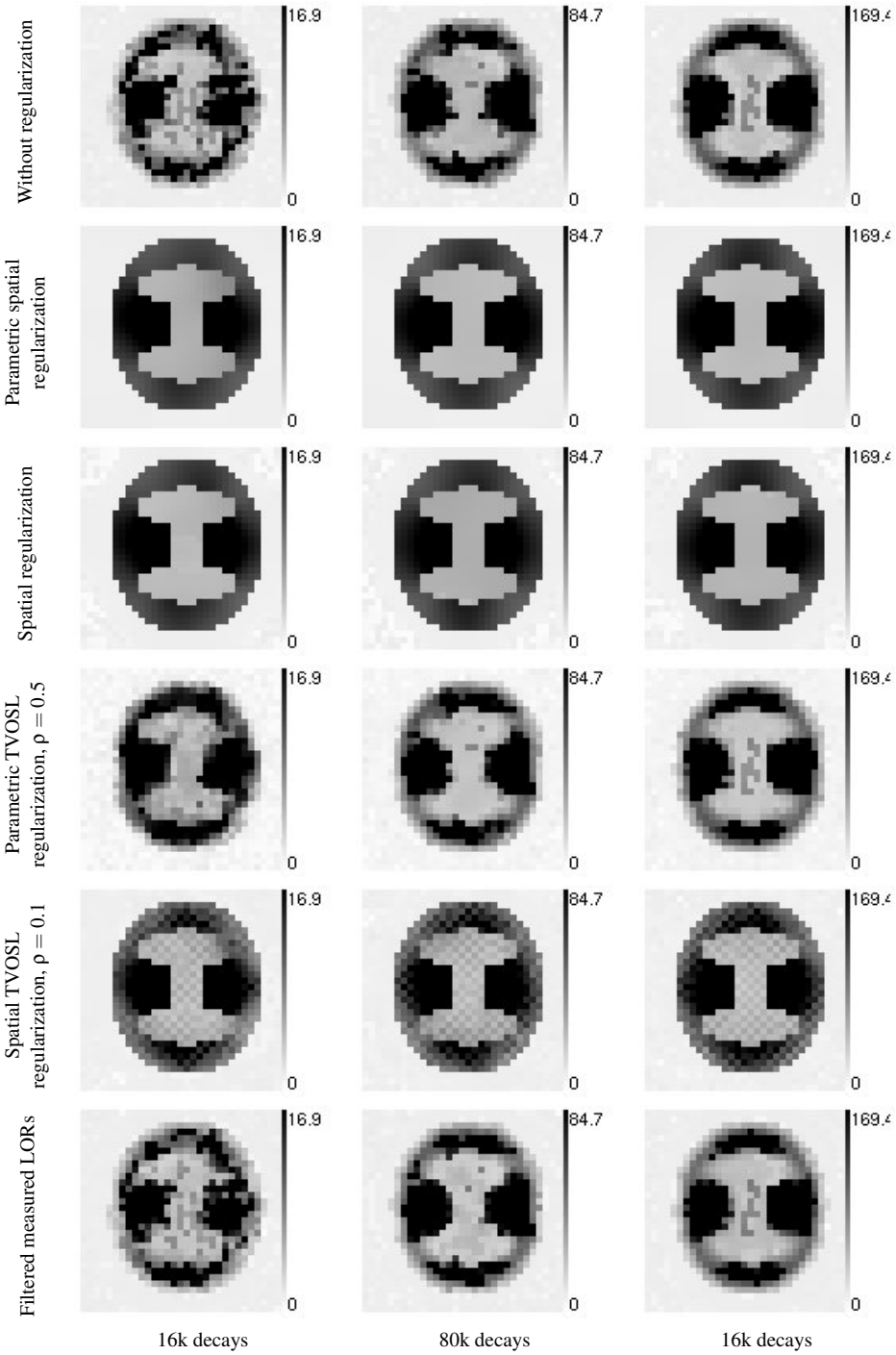

Figure 11: *Examples of reconstructed spatial activity at* $t = 1$.

positron emission tomography. *Phys. Med. Biol.*, 54:7379–400, 2009.

2. B. Csébfalvi. An evaluation of prefiltered reconstruction schemes for volume rendering. *IEEE Transactions on Visualization and Computer Graphics*, 14(2):289–301, 2008.
3. B. Csébfalvi. An evaluation of prefiltered B-spline reconstruction for quasi-interpolation on the body-centered cubic lattice. *IEEE Transactions on Visualization and Computer Graphics*, 16(3):499–512, 2010.
4. B. Csébfalvi. Cosine-weighted B-spline interpolation: A fast and high-quality reconstruction scheme for the body-centered cubic lattice. *IEEE Transactions on Visualization and Computer Graphics*, 19(9):1455–1466, 2013.
5. M.E. Kamasak, C.A. Bouman, E.D. Morris, and K. Sauer. Direct reconstruction of kinetic parameter images from dynamic pet data. *Medical Imaging, IEEE Transactions on*, 24(5):636–650, May 2005.
6. M. Magdics and et al. TeraTomo project: a fully 3D GPU based reconstruction code for exploiting the imaging capability of the NanoPET/CT system. In *World Molecular Imaging Congress*, 2010.
7. M. Magdics and et al. Performance Evaluation of Scatter Modeling of the GPU-based "Tera-Tomo" 3D PET Reconstruction. In *IEEE Nuclear Science Symposium and Medical Imaging*, pages 4086–4088, 2011.
8. M. Magdics, L. Szirmay-Kalos, B. Tóth, and T. Umenhoffer. Fast positron range calculation in heterogeneous media for 3D PET reconstruction. In *IEEE Nuclear Science Symposium Conference Record (NSS/MIC)*, 2012.
9. M. Magdics, L. Szirmay-Kalos, B. Tóth, and T. Umenhoffer. Filtered sampling for PET. In *IEEE Nuclear Science Symposium Conference Record (NSS/MIC)*, 2012.
10. Milán Magdics and László Szirmay-Kalos. *Optimization in Computer Engineering - Theory and Applications*, chapter Total Variation Regularization in Maximum Likelihood Estimation. Scientific Research Publishing, 2011.
11. Milán Magdics, Balázs Tóth, Balázs Kovács, and László Szirmay-Kalos. Total variation regularization in PET reconstruction. In *KÉPAF*, pages 40–53, 2011.
12. Milán Magdics and László Szirmay-Kalos. *Optimization in Computer Engineering*, chapter Total Variation Regularization in Maximum Likelihood Estimation, pages 155–168. Scientific Research, 2011.
13. László Papp, Gábor Jakab, Balázs Tóth, and László Szirmay-Kalos. Adaptive bilateral filtering for PET. In *IEEE Nuclear science symposium and medical imaging conference*, MIC'14, pages M18–104, 2014.
14. M. Persson, D. Bone, and H. Elmqvist. Total variation norm for threedimensional iterative reconstruction in limited view angle tomography. *Physics in Medicine and Biology*, 46(3):853–866, 2001.
15. G. Rácz and B. Csébfalvi. Tomographic reconstruction on the body-centered cubic lattice. In *Proceedings of Spring Conference on Computer Graphics (SCCG)*, 2015.
16. L. Shepp and Y. Vardi. Maximum likelihood reconstruction for emission tomography. *IEEE Trans. Med. Imaging*, 1:113–122, 1982.
17. Eddy T.P. Slijpen and Reek J. Beekman. Comparison of post-filtering and filtering between iterations for SPECT reconstruction. *IEEE Trans. Nuc. Sci.*, 46(6):2233–2238, 1999.
18. Donald L. Snyder and M.I. Miller. The use of sieves to stabilize images produced with the em algorithm for emission tomography. *IEEE Transactions on Nuclear Science*, 32(5):3864–3872, Oct 1985.
19. Donald L. Snyder, M.I. Miller, Lewis J. Thomas, and D.G. Politte. Noise and edge artifacts in maximum-likelihood reconstructions for emission tomography. *IEEE Transactions on Medical Imaging*, 6(3):228–238, Sept 1987.
20. L. Szirmay-Kalos. *Monte-Carlo Methods in Global Illumination — Photo-realistic Rendering with Randomization*. VDM, Verlag Dr. Müller, Saarbrücken, 2008.
21. L. Szirmay-Kalos, M. Magdics, and B. Tóth. Multiple importance sampling for PET. *IEEE Trans Med Imaging*, 33(4):970–978, 2014.
22. L. Szirmay-Kalos, M. Magdics, B. Tóth, and T. Bükki. Averaging and Metropolis iterations for positron emission tomography. *IEEE Trans Med Imaging*, 32(3):589–600, 2013.
23. L. Szirmay-Kalos, B. Tóth, and G. Jakab. Efficient Bregman iteration in fully 3d PET. In *IEEE Nuclear science symposium and medical imaging conference*, MIC'14, 2014.
24. László Szirmay-Kalos, Milán Magdics, and Balázs Tóth. Volume enhancement with externally controlled anisotropic diffusion. *The Visual Computer*, pages 1–12, 2016.
25. László Szirmay-Kalos, Balázs Tóth, and Milán Magdics. *GPU Computing Gems*, chapter Monte Carlo Photon Transport on the GPU, pages 234–255. Morgan Kaufmann Publishers, 2010.
26. V. Vad, B. Csébfalvi, P. Rautek, and E. Gröller. Towards an unbiased comparison of CC, BCC, and FCC lattices in terms of prealiasing. *Computer Graphics Forum (Proceedings of EuroVis)*, 33(3):81–90, 2014.
27. Eugene Veklerov and J. Llacer. The feasibility of images reconstructed with the methods of sieves. *IEEE Transactions on Nuclear Science*, 37(2):835–841, Apr 1990.
28. G. Wang and J. Qi. Direct estimation of kinetic parametric images for dynamic pet. *Theranostics*, 3(10):802–815, 2013.
29. Guobao Wang and Jinyi Qi. An optimization transfer algorithm for nonlinear parametric image reconstruction from dynamic pet data. *Medical Imaging, IEEE Transactions on*, 31(10):1977–1988, Oct 2012.
30. Jianhua Yan, Beata Planeta-Wilson, and R.E. Carson. Direct 4d list mode parametric reconstruction for pet with a novel em algorithm. In *Nuclear Science Symposium Conference Record, 2008. NSS '08. IEEE*, pages 3625–3628, Oct 2008.